NAIC-ID(RS)T-0516-95

NATIONAL AIR INTELLIGENCE CENTER

THE EFFECT OF TURBULENT OUTER SCALE ON ATMOSPHERIC TRANSVERSE COHERENCE LENGTH AND ISOPLANATIC ANGLES

by

Song Zhengfang, Fan Chengyu

Approved for public release: distribution unlimited

HUMAN TRANSLATION

NAIC-ID(RS)T-0516-95 28 Dec 95

MICROFICHE NR: 96C000002

THE EFFECT OF TURBULENT OUTER SCALE ON ATMOSPHERIC TRANSVERSE COHERENCE LENGTH AND ISOPLANATIC ANGLES

By: Song Zhengfang, Fan Chengyu

English pages: 20

Source: Qiangjiguang Yu Zizishu (High Power Laser and Particle Beams), Vol. 6, Nr. 3, August 1994; pp. 1; 337-381; 469-473

Country of origin: China
Translated by: SCITRAN
F33657-84-D-0165
Requester: NAIC/TATD/Bruce Armstrong
Approved for public release: distribution unlimited.

GRAPHICS DISCLAIMER

All figures, graphics, tables, equations, etc. merged into this translation were extracted from the best quality copy available.

ABSTRACT Based on the measured altitude distributional data of the turbulence structure constant (C_n^2), this article analyzes the effects of turbulent outer scale Lo on atmospheric transverse coherence length ro and isoplanatic angle Θo under the two conditions of large apertures and small apertures. Calculation results clearly show that, under conditions where Lo is a limited value, ro and Θo clearly increase. With regard to large aperture telescopes, in infrared wave bands--for example, wave lengths of 2.2 microns--ro and Θo are even larger. Θo can even reach 0.5 mrad.

KEY WORDS Turbulent outer scale Atmospheric transverse coherence length Isoplanatic angle

1 INTRODUCTION

Atmospheric coherence length ro and isoplanatic angle Θo are two important parameters describing spacial coherence characteristics associated with light wave propogation in turbulent atmospheres. Beginning in 1968, after Fried [1] put forward the concept of coherence length, it was universally accepted by academic circles. In recent years, research associated with ro and Θo has grown more dynamic. It has already spread from the realm of laser transmission to the world of astronomy. The source of the impetus lies in broad applications associated with adaptive optical technology (AOT). As is widely known, AOT is capable of compensating for coherence characteristic degnerative regression associated with light waves when they pass through the atmosphere. Moreover, the compensation effects are directly related to ro and Θo . As a result, theory developing ro and Θo as well as experimental research are very important.

It is generally thought that, in astronomical observations and measurements, within the range of visible light--ro = 2-20cm and Θo being 5-20microrad--when telescope apertures D are smaller than ro , the resolution of star images is limited by the telescope. When D is larger than ro , resolutions are limited by the atmosphere. In recent years, following along with theory and experimental work associated with in depth development, there are different ways of looking at this. This is primarily the discovery of atmospheric turbulence scale Lo above boundary layers. This certainly does not seem like the assumed several tens to several thousand meter ranges in traditional theories, but are relatively smaller. If Lo is actually relatively small, large aperture telescope resolutions will be greatly improved. In infrared wave bands, it is even possible to reach 0.05micorrad. At the present time, experiments have already clearly shown that--opting for the use of wave lengths of 2.2 microns--it is possible to reach resolutions which are 0.25microrads [2]. Recently, Coulman and others [3,4] made use of balloon borne high altitude sounding instruments and star light scintillation technology. In France, the U.S., and Chile carried out wide ranging measurements, guaging Lo values to be 30 - 40cm. Although, in the vicinity of the top of the troposphere, Lo was measured as approximately 5m, these amounts, however, are not adequate to influence averages associated with the atmosphere as a whole. McKechnie [2,5] believes that atmospheric trubulence is primarily located within altitudes 4-5km from the ground. Lo associated with the atmosphere as a whole are only 30-40cm. Atmospheric sounding data taken from Kunming clearly shows that Lo agrees with the measurements of Coulman and others in order of magnitude. As a result, it is then necessary to have the effects of finite turbulent outer scales on atmospheric coherence lengths and isoplanatic angles to carry out research.

2 WAVE STRUCTURE FUNCTIONS

/470

In traditional theory, when calculating wave structure functions, one generally opts for the use of Kolmogorov turbulence spectra. In this type of model, it is believed that Lo is quite large, with the result that it may not be considered. Now, through the measurements of Coulman and others as well as our measurements and calculations, it was discovered that Lo is relatively small. The equivalent Lo for the atmosphere as a whole is less than 1m. As a result, when calculating wave structure functions, it is necessary to make some corrections to Kolmogorov spectra. If one opts for the use of deformation Von Karman spectra

$$\Phi_n(K) = 0.033\, C_n^2 (K^2 + K_0^2)^{-11/6} \exp\left(-\frac{K^2}{K_m^2}\right) \tag{1}$$

Here, K is the spacial wave number. The unit is m-1 . Ko = 1/Lo. Km = 5.92/lo . lo is turbulent flow inner scale. C_n^2 is a characteristic turbulent flow strength index of refraction structural constant. The unit is m-2/3 . Then, wave structure constants [7] are

$$D(\rho, z) = 8\pi^2 k^2 \int_0^\infty dz \int_0^\infty [1 - J_0(K, \rho)] \Phi_n(K) K\, dK \tag{2}$$

In the equations, Φn (K) must make use of equation (1) for substitution. Moreover, k=2π/λ. λ is wave length. Jo (x) is a zero order Bessel function. ρ is the distance between the two points considered. In order to make calculations convenient, take Φn (K) and write it as Φn (K) = Φno (K) - Φ1 (K, Lo) - Φ2 (K, Lo, lo). Here, there is no relationship between Φno (K) and Lo or lo , that is, Kolmogorov spectra. Φ1 stands for the influence of Lo .

Φ2 stands for the influences associated with lo .

(3) $$\Phi_{n0}(K) = 0.033\, C_n^2 K^{-11/3}$$

(4) $$\Phi_1(K, L_0) = 0.033\, C_n^2 [K^{-11/3} - (K^2 + K_0^2)^{-11/6}]$$

(5) $$\Phi_2(K, L_0, l_0) = 0.033\, C_n^2 K^{-11/3} [1 - \exp(-\frac{K^2}{K_m^2})]$$

In equation (6), the influences of Lo on Φ2 are ignored. Going through detailed analysis, it is possible to finally obtain [6] $\rho < lo$. One has

(6) $$D(\rho, z) = 3.28 k^2 \rho^2 \int_0^\infty \frac{C_n^2}{l_0^{1/3}}\, dz$$

For $lo < \rho < Lo$, one has

(7) $$2.91 k^2 \rho^{5/3} \int_0^\infty C_n^2 [1 - 0.8048 (\frac{\rho}{L_0})^{1/3}]\, dz$$

For Lo < ρ, one has

$$1.563k^2\int_0^{\infty} C_n^2 L_0^{5/3}\,dz \tag{8}$$

In equation (8), when Lo is relatively large, (ρ/Lo) -> O. It is possible to use Kolmogorov spectra to derive

$$D(\rho, z)=2.91k^2\rho^{5/3}\int_0^{\infty} C_n^2 dz.$$

3 INFLUENCES OF OUTER SCALE Lo ON ro AND Θo

Use was made of balloon borne atmospheric sounding data taken at Kunming by Zeng Zongyong of the Academia Sinica Anhui Photomechanical Institute and others in order to analyze the influences of Lo on ro and Θo . Below, considerations are divided between two cases. One case is lo < ρ < Lo . The other is ρ > Lo. Through another type of expression for wave structure functions [1] /471

$$D(\rho)=6.88\left(\frac{\rho}{r_0}\right)^{5/3} \tag{9}$$

Making equations (7) and (8) respectively equal to equation (9), it is then possible to obtain (when lo < Θ < Lo and ρ > Lo) changes in ro following along with Lo . Then, from the relationship [8] Θo = 0.314ro /Ho it is then possible to solve for corresponding Θo values. At this time, atmospheric equivalent altitudes $H_0=[\int C_n^2(z)z^{5/3}dz/\int C_n^2\cdot(z)dz]^{3/5}$.

Below, respective consideration is given to these two types of cases.

(1) lo < ρ < Lo . Take ρ = 0.12m. From equations (7) and (9), one gets

$$r_0=\{0.423k^2\int_0^{\infty} C_n^2[1-0.8048\left(\frac{\rho_1}{L_0(z)}\right)^{1/3}]\,dz\}^{-3/5} \tag{10}$$

The altitude distribution associated with Lo is taken to be a type of charted formula (see Fig.1) based on data

measured in Chile [3]

$$L_0(z) = 0.5 + 5\exp\left(-\frac{z-7500}{2500}\right)^2 \quad (11)$$

In the equation, Lo and z units are, respectively, meters and thouands of meters.

Fig.1

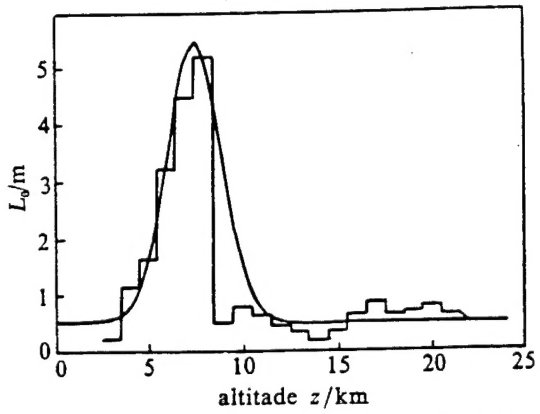

Fig.1 The height distribution of turbulent outer scale

To make comparisons, using the formulae derived in association with Kolmogorov spectra

$$r_0 = [0.423 k^2 \int_0^\infty C_n^2(z)dz]^{-3/5}$$

$$\theta_0 = [2.91 k^2 \cdot \int_0^\infty C_n^2(z) z^{5/3} dz]^{-3/5},$$

to make calculations, the calculation results for the two instances are seen in Tables 1A and 2.

(2) ρ > Lo . Take ρ = 8m. From equations (8) and (9), one gets the equation below (for calculation results, see Table 1B).

$$r_0 = \{0.227 k^2 \int_0^\infty C_n^2(z)(L_0(z))^{5/3} dz\}^{-3/5} \rho \quad (12)$$

TABLE 1

Table 1 The calculated values of r_0 and θ_0 for Von Karman spectrum

A. $\rho = 0.12$m B. $\rho = 8$m

time \ λ/μm	r_0/cm		θ_0/μrad		r_0/cm		θ_0/μrad	
	0.55	2.2	0.55	2.2	0.55	2.2	0.55	2.2
11－28－09	7.8	37.1	2.18	11.49	30.7	162.1	9.51	50.18
11－28－15	5.6	29.4	2.56	13.54	24.7	130.6	11.39	60.13
11－29－07	20.0	105.5	8.64	45.63	166.7	879.7	72.09	380.50
11－29－19	24.1	127.4	10.78	56.91	149.0	786.5	66.56	351.30
11－29－23	20.9	110.5	11.99	63.29	167.4	883.5	25.90	506.16
11－30－16	17.7	93.3	5.49	28.99	88.4	466.8	27.49	145.10

"11－28－09" means at 9am. on Nov. 28, 1992.

TABLE 2

Table 2 The calculated values of Kolmogorov spectrum

$\rho = 0.12$m

r_0/cm		θ_0/μrad	
0.55	2.2	0.55	2.2
5.2	27.6	1.62	8.54
4.4	23.2	2.02	10.67
13.8	72.6	5.96	31.45
17.3	91.2	7.73	40.81
14.5	76.4	8.30	43.79
12.9	68.0	4.01	21.17

6a 7

4 CONCLUSIONS /472

Considering the influences associated with turbulent outer scale Lo, use was made of expressions for ro and Θo derived with Von Karman spectra. Making use of empirically measured C_n^2 vertical distribution data, calculations were carried out with regard to ro and Θo . From the calculation results, it was discovered that, after considering the influences of Lo , ro and Θo clearly increase. In the past, it was generally believed that there was practically no difference between the performance of large
aperture telescopes due to atmospheric turbulence and small aperture telescopes of 10-20cm. Now, considering Lo effects, estimates are much larger making use of large aperture telescope ro and Θo than using traditional theories. In particular, in the infrared wave length--for a 2.2 micron aperture, for instance--it is 8m, and Θo is capable of reaching approximately 0.5mrad. With regard to tracking and guidance, this is capable of having a much larger selection domain. ro is capable of increasing to being equivalent to apertures in contact. In this way, the receiving system is capable of possessing optimum properties [9]. In this type of case, adaptive optical technology is, perhaps, unnecessary, or adaptive optical systems with relatively low indices are also capable of satisfying requirements. We expect that this conclusion can be experimentally verified.

REFERENCES

1 Fried DL. *Proc IEEE*, 1967, **55**: 57

2 McKechnie TS. *J. Opt Soc Am*, 1992, **A9** : 1937

3 Coulman CE, *et al*, *Appl Opt*, 1988, **27**: 155

4 Coulman CE and Vermin *J. Appl. Opt*, 1991, **30**: 118

5 McKechnie TS. *J. Opt Soc*, *Am* 1991, **A8**: 346

6 Strohbehn JW. Laser Beam Propagation in the Atmosphere. (Topics in applied physics; v. 25) New York 1978

7 Tatarski VI. 湍流大气中波的传播理论. 北京: 科学出版社, 1978

8 Loos GC and Hogge CB, *Appl Opt*. 1979, **18**: 2654

9 Fried DL. *J. Opt Soc Am*, 1965, **55**: 1427

NAIC-0516-95.2 /373

NUMERICAL SIMULATIONS OF TRANSIENT THERMAL BLOOMING EFFECTS

Zhang Tianshu Lei Guangyu Xie Lijuan

Translation of "Re Yun Shun Tai Xiao Ying De Shu Zhi Mo Ni", HIGH POWER LASER AND PARTICLE BEAMS, Vol.6, No.3, Aug 1994, pp 373-382

Translated by

S C I T R A N

1482 East Valley Road

Santa Barbara, CA 93108

ABSTRACT On the basis of transient state four dimensional (4D) thermal blooming programs, this article studies transient thermal blooming effects during atmospheric laser transmission as well as how they transition to thermal blooming states under isobar approximation. In conjunction with this, comparisons are made with 4D thermal blooming program calculation results under isobar approximation. At approximately four fold fluid dynamic time scale (4th), transient 4D thermal blooming program calculation results are close to results under isobar approximation. Besides that, phase compensation calculations were also done. In cases with light intensities of a few kW/cm2, under ideal adaptive optical system kinetic conditions, transient phase thermal distortions are capable of being compensated for in real time relatively effectively.

KEY WORDS Transient thermal blooming Isobar approximation Phase compensation

I. BASIC EQUATIONS

Thermal blooming effects are limitations on laser strengths passing through the atmosphere, giving rise to nonlinear phenomena associated with beam distortions. Due to the fact that the details of theoretical research outside China on thermal blooming effects during the full course of laser transmission in the atmosphere have still not been made public, as a result, there is a great need for research on laser thermal blooming effects during the whole process in the atmosphere as well as for the establishment of 4D thermal blooming programs. This article lays stress on the description of transient effects in order to facilitate an understanding of whether or not transient distortions are capable of effective real time compensation. In conjunction with this, observations are done of the effectiveness of isobar approximations. Use is made of computer numerical values to describe basic equations associated with thermal blooming of the several types below.

1.1 Field Equations

Using monochromatic, linear polarized scalar wave motion equations to describe laser fields--under asymptotic approximation--in following the wave motion coordinate system, the slowly changing field propogated in the positive Z direction satisfies the equation below

$$2ik\frac{\partial\psi}{\partial Z}+\nabla_{\perp}^{2}\psi+k^{2}\delta\varepsilon(\psi,t)\psi=0 \qquad (1)$$

In this, $k=2\pi/\lambda$. λ is laser wave length in a vaccuum. $\nabla_{\perp}^{2}$ is the Laplace operator associated with vertical light axses. $\delta\epsilon$ is diaelectric constant change.

As far as beacon light propogated in the negative Z direction is concerned, it has the equation below

/374

$$-2ik_{b}\frac{\partial\psi_{b}}{\partial Z}+\nabla_{\perp}^{2}\psi_{b}+k_{b}^{2}\delta\varepsilon_{b}\psi_{b}=0 \qquad (2)$$

Assuming that kb = k , $\delta\epsilon b = \delta\epsilon(\psi,t)$, and omiting delay effects, it is believed that beacon light is reverse propogated in a "distribution lens" created by laser emissions. Nonlinear Xue Dingwo equation (1) can use various types of methods for solution (integral transform methods, difference methods, as well as Green Function methods, and so on). In the processing below (with a $O(\Delta Z2)$ precision) using FFT methods to solve, one takes equation (1) and solves in terms of a form within a step length of ΔZ to get

$$\psi(Z+\Delta Z,\ r_{\perp},\ t)=\exp\left[i\left(\frac{\nabla_{\perp}^{2}}{2k}+\frac{k\overline{\delta\varepsilon}}{2}\right)\Delta Z\right]\psi(Z,\ r_{\perp},\ t) \qquad (3)$$

In this, $\overline{\delta\varepsilon}=\frac{1}{\Delta Z}\int_{z}^{Z+\Delta Z}\delta\varepsilon(Z')dZ'$. $r_{\perp}$ is the vertical

optical axis coordinate vector.

Equation (3) can be expressed as

$$\psi(Z+\Delta Z, r_\perp, t)=\exp[i(\frac{\nabla_\perp^2}{2k})\frac{\Delta Z}{2}]\exp[i(\frac{k\overline{\delta\varepsilon}}{2})\Delta Z\exp[i(\frac{\nabla_\perp^2}{2k})\frac{\Delta Z}{2}]\psi(Z, r_\perp, t) \quad (3')$$

When making use of equation (3'), it requires step length ΔZ to satisfy the condition below [1]

$$\frac{k}{2}\overline{\delta\varepsilon}\Delta Z \ll 1 \quad (4)$$

As far as using the following structural relationships as well as density changes in isobar approximations are concerned, with regard to propogation calculations for laser beams with wave lengths of 1 micron, it is necessary for step length ΔZ to satisfy

$$\Delta Z/\mathrm{cm} \ll \frac{10^{-4}}{|\rho_1|}=2.5\times10^{-8}\frac{1}{\alpha_a/(\mathrm{cm}^{-1})I_p/(\mathrm{MWcm}^{-2})\cdot t/\mathrm{s}} \quad (4')$$

In this relationship, αa is the absorption coefficient. Ip is peak value light strength. t is time.

Obviously, $\exp[i(\frac{\nabla_\perp^2}{2k})\frac{\Delta Z}{2}]\psi(Z, r_\perp, t)$ in equation (3') is a solution in the back half of step lengths for Z in the vaccuum wave motion equation below

$$2ik\frac{\partial\psi}{\partial Z}+\nabla_\perp^2\psi=0 \quad (5)$$

The effects of dielectric media are equivalent to phase multiplication factor $\exp[i(\frac{k}{2})\overline{\delta\varepsilon}\Delta Z]$. In the fields obtained, use is then made of operator $\exp[i(\frac{\nabla_\perp^2}{2k})\frac{\Delta Z}{2}]$ to act on them. This is equivalent to taking the obtained fields (in $Z+\frac{\Delta Z}{2}$ locations) and making "initial" conditions on the bottom half of step lengths to solve vaccuum wave motion equations. In this way, one gets a step length field. In the same way, step lengths are solved for, one after the other (called multiple phase screen treatment), that is, it is possible to solve for fields at different propogation distances.

As far as solving for vaccuum wave motion equations in configurational space is concerned, in solutions, there are

contained second degree differential operators $\nabla_\perp^2 (= \frac{\partial^2}{\partial x^2} + \frac{\partial^2}{\partial y^2})$

Moreover, going through Fourier transforms (equivalent to $\nabla_\perp^2 \to -(k_x^2+k_y^2)$) to transform into solution field spectra in "spacial frequency" space, then, from equation (5), one has

$$\tilde{\psi}(Z+\Delta Z, k_x, k_y)=\exp[-\frac{1}{2k}(k_x^2+k_y^2)\Delta Z]\tilde{\psi}(Z, k_x, k_y) \qquad (6)$$

Here, $\tilde{\psi}$ is the Fourier transform associated with ψ, that is,

/375

$$\tilde{\psi}(Z, k_x, k_y)=\iint_{-\infty}^{\infty}\psi(Z, r_\perp)\exp(-ik\cdot r_\perp)dr_\perp$$

$$=\iint_{-\infty}^{\infty}\psi(Z, X, Y)\exp[-i(k_xX+k_yY)]dxdy$$

Besides this,

$$\psi(Z, X, Y)=\frac{1}{(2\pi)^2}\iint_{-\infty}^{\infty}\tilde{\psi}(Z, k_x, k_y)\exp(ik\cdot r_\perp)dk_xdk_y$$

In the two types of spaces, dispersion is carried out. In conjunction with this, application is made of periodic boundary conditions to obtain

$$k_x=\frac{2\pi}{L_x}m \quad , \quad k_y=\frac{2\pi}{L_y}n$$

In this, m,n=-N/2...1,2,... N/2 and Lx, Ly are function periods in the two directions. Choosing the two to be equal, it is necessary to point out that, if functional transverse distributions in configurational space are steep, then, there should be a great many modes contained in "spacial frequency" space. As a result, N is taken to be very large, and configurational space coordinate dispersion shows

$$X_j=j\Delta X \quad , \quad Y_l=l\Delta Y$$

In this, j,l=0,1,... N-1. Taking transverse step lengths $\Delta X=\Delta Y=L/N$, application is made of the various equations above. Then, equation (6) becomes

$$\tilde{\psi}_{mn}(Z+\Delta Z)=\exp[-\frac{i}{2k}(\frac{2\pi}{L})^2(m^2+n^2)\Delta Z]\tilde{\psi}_{mn}(Z) \qquad (6')$$

Going through reverse Fourier transformation, it is then possible to obtain configurational fields in space $\psi(Z+\Delta Z, X_j, Y_l)$. Thus, optical strengths

$$I(Z+\Delta Z, X_j, Y_l)=\frac{c}{8\pi}\psi\psi^*(Z+\Delta Z, X_j, Y_l) \qquad (7)$$

Giving consideration to linear absorption and scattering, there is a need to introduce attenuation operators

$$\exp[-\int_{z}^{z+\Delta z}\alpha_t(Z')dZ'\ ],$$

$\alpha t = \alpha s + \alpha a$. αa and αs are, respectively, absorption and scattering coefficients.

1.2 Fluid Dynamic Equation Sets

Due to the fact that atmospheric laser absorption for wave lengths that interest us is very weak, during laser transmission, it leads to atmospheric status parameter changes being very small. It is possible to opt for the use of linearized fluid dynamic equation sets to describe changes in atmospheric configuration parameters, that is,

$$\frac{d\rho_1}{dt} + \rho_0 \nabla \cdot \boldsymbol{u} = 0 \qquad (8a)$$

$$\rho_0 \frac{d\boldsymbol{u}}{dt} = -c_1^2 \nabla p_1 \qquad (8b)$$

$$c_2^2 \frac{dp_1}{dt} - c_3^2 \frac{d\rho_1}{dt} = (r-1)\alpha_a I_p = S \qquad (8c)$$

In these, because pressure p1 units make use of atm(latm=101.325kPa) and optical strength Ip units make use of MW.cm-2 , and, due to introduced unit transformation operators $c_1^2 = 1.0133 \times 10^6,\ c_2^2 = 0.10133 \times 10^{-6},\ c_3^2 = 10^{-13} c_*^2,$, r is an adiabatic index, and Ip does not depend on time t. It is possible to obtain scattering spectra associated with density changes and pressure changes in "spacial frequency" space

$$\tilde{\rho}_{1mn}(Z,t) = -\frac{\tilde{S}_{mn}(Z)}{c_3^2} t[1 - \frac{\sin(wt\sqrt{m^2+n^2})}{wt\sqrt{m^2+n^2}}] \qquad (9)$$

/376

$$\tilde{p}_{1mn}(Z,t) = \frac{\tilde{S}_{mn}(Z)}{c_2^2 w\sqrt{m^2+n^2}} \sin(wt\sqrt{m^2+n^2}) \qquad (10)$$

In this, $w = \frac{c_1 c_3}{c_2}\ \frac{2\pi}{L} = c_s \frac{2\pi}{L}$, and

$$\tilde{S}_{mn}(Z) = (r-1)\alpha_a \exp[-\int_0^Z \alpha_t(Z')dZ']\,\tilde{I}_{pmn}(Z) \qquad (11)$$

Doing reverse Fourier transforms, it is possible to obtain ρ1 and p1 on scattering points in configurational space

$$\rho_1(Z, j\Delta x, l\Delta y, t) = \sum_{m,n=-N/2}^{n/2} \sum^{-1} \tilde{\rho}_{1mn}(Z,t) \exp[i\frac{2\pi}{N}(mj+nl)] \qquad (12)$$

$$p_1(Z, j\Delta x, l\Delta y, t) = \sum_{m,n=-N/2}^{n/2} \sum^{-1} \tilde{p}_{1mn}(Z,t) \exp[i \frac{2\pi}{N}(mj+nl)] \qquad (13)$$

Applying ideal gas configuration equations, it is possible to obtain temperature changes

$$T_1(Z, j\Delta X, l\Delta Y, t) = \frac{p_1}{\rho_0 \Gamma} - T_0 \frac{\rho_1}{p_0} \qquad (14)$$

In this, Γ=2.848 atm.cm3/K.g.

From equation 8(c), it is known that isobar conditions correspond to c2 = 0. When Ip does not depend on time t, integrating t, one gets density changes associated with isobar conditions

$$\tilde{\rho}_{1p}(Z, X, Y, t) = -\frac{t}{c_3^2} S(Z, X, Y) \qquad (15)$$

This and the results in reference [2] are the same. Making Fourier transforms with regard to equation (15), scattering gives one

$$\rho_{1mnp}(Z, X, Y, t) = -\frac{t}{c_3^2} S_{mn}(Z) \qquad (16)$$

This is precisely the first term on the right side of equation (9). From this, it is possible to know that transient correction terms at nonisobaric times are precisely the second term contained in square brackets on the right side of equation (9). They follow increases in t and decrease. Moreover, high frequency mode contributions follow increases in t and attenuate even faster. With regard to Gaussian distributions, low frequency modes account for the dominent positions. In this way, when Xm = 10, from sinX/X -> 0, it is then possible to estimate that transient contribution attenuation times are a few fluid dynamic time periods (Here, fluid dynamic time scales tH = a/cs. a is optical strength e-2 beam radii. Taking transverse function period L=6a, attenuation time period $t_d = X_m t_H / \sqrt{m^2+n^2}$.). Besides that, from equations containing source sound waves, it is also possible to derive this transient term. From (8a - 8c), it is known that,

$$\frac{\partial}{\partial t}(\nabla_\perp^2 - \frac{1}{c_s^2}\frac{\partial^2}{\partial t^2})\rho_1 = -\frac{r-1}{c_3^2}\alpha_a \nabla_\perp^2 I_p \qquad (17)$$

Isobar approximations correspond to the speed of sound cs -> ∞, that is, distrubances in the development of infinite speeds, instantaneously bringing them to the same level, when Ip does not depend on time t. From equation (17), it is possible to obtain--under isobar--density $\rho_{1p} = -\frac{r-1}{c_3^2}\alpha_a I_p t$. . This is the same as equation (15). In early periods, ρ1 transverse changes are small. $\nabla_\perp^2 \rho_1 \to 0$, . When Ip does not depend on time t, it is possible, from equation (17), to obtain density variations

associated with t3 thermal blooming phases

$$(\rho_1)_{t^3b}=\frac{t^3}{3!}(r-1)\alpha_a(\nabla_\perp^2 I_p)\frac{c_s^2}{c_3^2} \tag{18}$$

Normally, wind speed vw << cs . Thus, wind transit periods are far longer than fluid dynamic time scales tH . As a result, thermal blooming phenomena within fluid dynamic time period scales for research are capable of not figuring in the influences of wind. In this way, equation (17) is axially symmetrical. /377 When Ip does not depend on time t, it is possible to go through Han Keer transforms, and that will do. With regard to second order ordinary differential equations associated with $\partial\rho_1/\partial t$, use is made of initial conditions $\rho_1(t=0,\ r_\perp)=\frac{\partial\rho_1}{\partial t}$ $(t=0,\ r_\perp)=0$. It is possible to obtain

$$\rho_1(t,r_\perp,z)=-\frac{r-1}{c_3^2}\alpha_a[I_p(r_\perp,z)t-\frac{1}{c_s}\int_0^\infty \tilde{I}_p(t)\sin(c_s\lambda t)*J_0(\lambda r_\perp)d\lambda \tag{19}$$

In early periods, it is thought that Ip does not undergo thermal blooming effects. It is possible to adopt $I_p(r_\perp,z)=I_p^0\exp$ $(-2|r_\perp|^2/a^2)$, . Making Han Keer transformations, one obtains

$$\tilde{I}_p(\lambda)=\frac{I_p^0}{4}a^2\exp(-\frac{\lambda^2a^2}{8})$$

On optical axses, $r_\perp$ = O. Thus, zero order Bessel function Jo = 1. Because of this, at a relatively early time, from equation (19), one obtains

$$\rho_1(t,r_\perp=0,Z)=-\frac{r-1}{c_3^2}\alpha_a I_p^0(t-\frac{t_H^2}{4t}) \tag{20}$$

From this, it can be seen that a few fluid dynamic time period transient portions are then attenuated away.

1.3 Structural Relationships

Structural relationships give the relationships between indices of refraction or dielectric constants and dielectric media configuration parameters. From reference [2], one knows that

$$n-1\approx\frac{3\times10^{-4}}{\rho_0}\rho=0.23\rho \tag{21}$$

From this, it is possible to obtain

$$\delta\varepsilon=2\delta n=0.46\rho_1(Z,X,Y,t) \tag{22}$$

2 CALCULATION RESULTS AND ANALYSES

(1) Definite Solution Conditions (Collimated beam, Gaussian transverse distribution)

$$Z=0,\ \psi(X,Y,Z=0)=\psi_0\exp(-\frac{X^2+Y^2}{a^2})$$

In this, $\psi_0 = 2.71 \times 10^4 \sqrt{I_p^0}$. If consideration is given to phase compensation, the right side multiplication factor

$$\exp\{-i\mathrm{tg}^{-1}[\frac{\mathrm{Im}\psi_b(X,Y,Z=0)}{\mathrm{Re}\psi_b(X,Y,Z=0)}]\},\ Z>0\quad X,Y\to\pm\infty,\ \psi\to 0,\ Z=L_{//},\ \psi_b(X,Y,Z=L_{//})=\psi_{b0}\exp(-\frac{X^2+Y^2}{a^2})$$

In this, $L_{//}$ is laser emission transmission distance. t = O. ρ1 = p1 = u = O. (2) Atmospheric Model $\rho(Z)\propto e^{-bz}$, b = 0.143x10-5cm1. (3) Parameters Used λ = 1 micron, αa(Z=O)=0.12x10-6cm-1, αt(Z=O)=0.12x10-6cm-1, r=1.4; cs = 330m/s.

Use was made of transient thermal blooming 4D programs (FFT methods) to do numerical value calculations on thermal blooming associated with different beam radii αo , different optical strengths I_p^0, , and different transmission distances $L_{//}$. Results are seen in the various tables or charts. For the sake of comparison, numerical value calculations associated with isobar approximations were done on certain models (Table 1). In conjunction with this, phase compensation calculations were made (Tables 3, 4).

From Fig.1, it can be seen that, when t < 2tH, pressure change radial distributions are basically pulled to the same level. After 4tH, an even status was maintained throughout. However, beam edge areas, by contrast, are higher than beam centers. This is due to the use of continuous wave Gaussian radial distribution lasers. In this way, center location pressure perturbation sources are maintained right along. Pressure disturbance waves are propogated toward beam edges. Due to "pursuing characteristic line" effects (characteristic line converegence), edge pressures are slightly higher than the center. Besides that, it is also possible to see that, with regard to beam center vicinity fixed spacial positions, pressure perturbation value time changes go up first. They do not reach tH and then begin to decline. When they reach the vicinity of 4tH, they do not decline any more. After that, they gradually go up again. The explanation of this is constant source perturbation. With regard to time scales being unable to form real isobar configurations, although pressure space distributions are capable of being pulled up to the same level, fixed point pressures, however, still follow along with increases in t and go up. This type of so called "isobar configuration" is, in fact, a superposition of a number of transient effects. Giving consideration to $\frac{\partial p_1}{\partial t}\Big|_{r_1} \neq 0$, , ρ1 will be smaller than equation (15) when at times of isobaric approximation (see Table 1 last column). /378

TABLE 1

表 1 $a=250$cm, $I_p=3.2$kW·cm^{-2}时由各方法所得的轴上参量

Table 1 The on axis parameters obtained by various methods

t/ms		$L_{\parallel}=3$km			5km			7km			10km		
		I_p	$-\rho_1$	p_1	I_p	$-\rho_1$	p_1	I_p	$-\rho_1$	p_1	I_p	$-\rho_1$	p_1
1.5 ($0.2t_H$)	A	2.60	1.100		2.30	0.710		2.10	0.490		1.90	0.290	
	B	2.60	0.056	1.1	2.3	0.038	0.76	2.1	0.026	0.53	1.90	0.016	0.32
	C		0.058			0.039			0.027			0.016	
3.75 ($0.5t_H$)	A	2.55	2.600		2.29	1.80		2.10	1.20		1.90	0.72	
	B	2.55	0.740	2.1	2.30	0.50	1.50	2.10	0.35	1.0	2.00	0.20	0.60
	C(18*)		0.900			0.61						0.25	
7.5 ($1t_H$)	A	2.55	5.20		2.30	3.50		2.00	2.40		1.80	1.40	
	B	2.55	3.80	2.00	2.30	2.40	1.30	2.00	1.70	0.90	1.90	0.95	0.55
	C												
15 ($2t_H$)	A	2.50	10.0		2.20	6.70		2.00	4.60		1.80	2.70	
	B	2.50	10.0	0.80	2.20	6.50	0.56	2.00	4.50	0.39	1.90	2.60	0.23
	C(15*)		12.0			8.10			5.60			3.30	
30 ($4t_H$)	A	2.49	21.0		2.00	13.0		1.90	9.60		1.60	4.80	
	B	2.49	21.0	0.39	2.00	12.0	0.26	1.80	8.40	0.18	1.50	4.50	0.11
	C(15*)		24.0			16.0			13.00			6.80	

Note : Calculation parameter $a=250$cm, $I_p^0=3.2$kW·cm^{-2}, I_p is in kW·cm^{-2}, pressure p_1 is in 10^{-6}atm, density ρ_1 is in 10^{-9}g·cm^{-3}, A is isobaric results, B is transient, C is analytical solutions (see eq. 18), * Digit after "C" is equation number.

From Table 1, it is possible to see that, at different transmission distances, changes in (-ρ1) as a function of t are basically in agreement with transient analysis results associated with equation (18) when t < tH/2. When t > 2tH , there is, basically, agreement with isobaric approximation results associated with equation (15). When the two really approach each other is after t > 4tH. On axis pressures follow changes in t not with monotomic rises to saturation values, but with decreases after first rising, and with continuous waves slowly going up. Extreme value time periods to, can be calculated from equation (8c). Adopting $\frac{dp_1}{dt}(t_0)=0$, thus,

$$\frac{d\rho_1}{dt}(t_0)=-\frac{1}{c_3^2}(r-1)\alpha_a I_p^0$$

Taking $I_p=I_p^0\exp(-2r_\perp^2/a^2)$, substitute into equation (18). In conjunction with that, when attention is paid to $r_\perp=0$, $\nabla_\perp^2 I_p=-\frac{8I_p^0}{a^2}$. Thus, $\frac{d\rho_1(t_0)}{dt}=-\frac{4I_p^0 t_0^2}{c_3^2 a^2}(r-1)\alpha_a$, . Because of this,

$$t_0=\sqrt{\frac{a^2}{4c_s^2}}=\frac{1}{2}t_H \qquad (23)$$

/379

Moreover, time periods when on axis pressure changes take extreme values associated with transient state 4D thermal blooming program calculation results are approximately 0.6tH. The two are basically in agreement. Rough estimate values for on axis maximum pressure changes at $L_{//}$ = 10km locations are $p_1(r_\perp=0, L_{//}=10\text{km}, t_0)=p_1(r_\perp=0, Z=0, t_0)\exp[-(b+\bar{a}_t)L_{//}]$ 5.66x10-7atm≈0.568Pa and are also in basic agreement with program calculation results. Here

$$\bar{\alpha}_t = \frac{\alpha_t(0)}{L_{//}} \int_0^{L_{//}} e^{-bZ} dZ = \frac{\alpha_t(0)}{bL_{//}} (1 - e^{-bL_{//}}) \qquad (24)$$

Table 2

Table 2 The results computed by transient thermal blooming code for various a, I_p^0 and $L_{//}$ at $4t_H$

a/cm	I_p^0	$L_{//}$/km	I_p	$-\rho_1$	p_1	$F=ka^2/L_{//}$	N_D
1	3.2	0.1	5.2	0.27	2.6	6.28	
	10		16	0.8	8.1		
	32		47	0.024	26		0.35
	320		257	0.0013	266		1.80
50	0.4	2	0.337	0.66	10.1	785	1.91
	3.2		2.43	0.048	81		13.9
	32		20.4	0.0040	810		111
250	3.2	3	2.49	0.0021	390	13090	91
		5	2.0	0.0012	260	7862	
		7	1.8	0.084	160	5616	
		10	1.5	0.045	110	3931	

Note : The phase compensation have been unstabilty when N_D is more than several hundreds then $N_D = 2\pi \int_0^{L_{//}} \delta n dz/\lambda$, $N_c = N_D/F$ (see proc SPIE Vol.1221), I_p^0, I_p are in kW · cm^{-2}, $-p_1$ is in 10^{-9}atm, ρ_1 is in 10^{-9}g · cm^{-3}.

/380

From Table 1, it is also possible to see that, with regard to fixed instants, ρ1 and p1 follow changes in transmission distances $L_{//}$ and are basically $\exp[-(b+a_t)L_{//}]$. Because ρ1 and p1 are in direct proportion to αIp, of course, if thermal distortion is severe, $I_p(L_{//}) \propto (-\bar{\alpha}_t L_{//}) \cdot \exp(-N_c)$. With regard to our case, distortion is weak, exp(-Nc)->1.

From Table 2, one knows that, no matter whether radii are large or small, optical strengths are high or low (within a certain limit), transmission distances are long or short, thermal distortion, when t ≤ 4tH, is very weak in all cases. Moreover, on axis optical strengths and I_p^0 form a

TABLE 3

Table 3 The calculation results for phase compensation (radial distribution of intensity)

No	65 ($r_\perp = 0$)	66 (12cm)	67 (24cm)	68 (36cm)	69 (36cm)	70 (36cm)
I_{pc}	1.78	1.77	1.75	1.71	1.65	1.58
I'_{pc}	1.97	1.96	1.94	1.90	1.84	1.76
I_g	3.2	3.19	3.14	3.08	2.98	2.87
I_u^*	1.972	1.966	1.935	1.898	1.837	1.769
No	71 (36cm)	72 (36cm)	73 (36cm)	74 (36cm)	75 (36cm)	76 (132cm)
I_{pc}	1.50	1.41	1.31	1.21	1.10	1.00
I'_{pc}	1.68	1.59	1.44	1.38	1.27	1.16
I_g	2.73	2.58	2.42	2.24	2.06	1.88
I_u^*	1.682	1.590	1.490	1.380	1.269	1.159

Note : "No" is radial coordinate, I_{pc} (I'_{pc}) is intensity without (or with) compensation, $I_g(r_\perp)$ is intensity of Gaussian distribution, I_u is intensity without blooming, all of intensity units are in $kW \cdot cm^{-2}$, $t = 4t_H = 30ms$, $L_{//} = 10km$, $a = 250cm$, $I_p^0 = 3.2kW \cdot cm^{-2}$, $I_a^* = I_g(r_\perp)e^{-2.1\times 10^0}$

direct proportion. This is extremely beneficial with regard to real time phase compensation.

In Table 3, thermal distortions associated with t ≤ 4tH phases are not great. Compensation is easy. Thermal distortion optical strength radial distributions deviate from Gaussian distributions. After going through phase compensation, 10km location optical strength radial distributions almost change into ideal Gaussian distributions.

From Table 4, it is possible to know that, no matter how early the time, at different transmission distances, very good compensation was obtained in all cases. Here are the calculations carried out with regard to continuous lasers. We have not yet done calculations for pulse lasers. Provided pulses are smaller than fluid dynamic time scales--basically belonging to t3 thermal blooming--it is possible to go through real time phase compensation, correcting transient thermal blooming distortion. With regard to pulse lasers, when pulse intervals are larger than or equal to wind transit periods, pulses series will not accumulate thermal distortions to a level which cannot be compensated for. Reference [3] already pointed out that single pulse and multiple pulse thermal blooming are both weaker than is the case with continuous wave lasers. Therefore, with regard to thermal blooming associated with pulse series laser beams, it seems even easier to make adaptive optical compensation in real time.

Fig.1

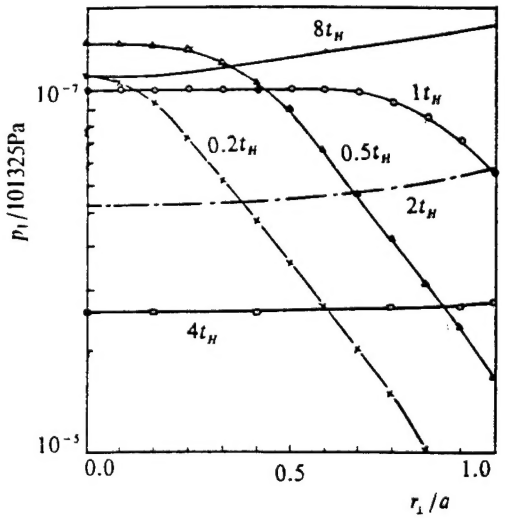

Fig 1 The radial distributions of pressure changes at various times when $L_{//}=100\text{m}$ ($a=1\text{cm}$, $I_p^0=32\,\text{kW}\cdot\text{cm}^{-2}$)

3 PRELIMINARY CONCLUSIONS

In order to save on computation time--time when computers are in use--spacial step lengths are relatively large. As a result, the precision of calculation results is not too high. However, a number of patterns revealed are still credible. The

reason is that field calculations in programs go through inspections of round vaccuum aperture refractive analysis results, and, in the programs, the ρ1 and p1 obtained from fluid dynamic calculations agree with rough analytical estimate values in cases of limitations. On the basis of the calculations above, it is possible to obtain the preliminary conclusions below:

(1) Transient effects, up to approximately 4tH times, basically approach quasi isobaric states. In the case of t < tH , one is placed in a t3 thermal blooming state. In the case of t ≥ 4tH , one basically reaches a quasi isobaric situation. When optical strength changes are not considered, density changes and time t form a direct proportion.

(2) Within the range of parameters which interest us, no matter how large or small a is, and, no matter how long or short 1 is or how high or low optical strengths are, provided one is within the period $t \leqslant 4t_H$, thermal distortions are all very weak. Thus, it is possible to realize relatively effective phase compensation. However, here, the effects of small scale /381 instabilities are not figured in. Moreover, phase compensation is ideal.

From transient 4D thermal blooming program calculation results, it is possible to predict that, with regard to laser thermal distortions for systems associated with pulses smaller than fluid dynamics periods tH it is possible to do real time phase compensation. Provided pulse intervals are larger than wind transit times--with regard to requirements associated with "optimum" characteristics of pulse interval structures--it seems to be possible to relax them. Moreover, in regard to pulse spacial structures, there is still a need for attention because, during t3 thermal blooming, $\rho_1 \propto \nabla^2 I_p$. As far as concrete conclusions are concerned, they await the next step in the detailed analysis of 4D thermal blooming program numerical value calculations concerning such effects as calculated turbulent flow, wind, and so on.

Acknowledgments The physical designs on which this work is based were supplied by Zheng Shaotang. Moreover, Zheng Shaotang and Lin Dewen provided invaluable opinions. For this, we give them our thanks.

REFERENCES

1 Brueckner KA. DE89 009919, 1987:10

2 Strohbehn JW. *Topics in Applied Physics*, 1978, **25**

3 Ulrich PB. AGARD Conference, NATO, 1972, (183):31 ~ 19

DISTRIBUTION LIST

DISTRIBUTION DIRECT TO RECIPIENT

ORGANIZATION	MICROFICHE
B085 DIA/RTS-2FI	1
C509 BALL0C509 BALLISTIC RES LAB	1
C510 R&T LABS/AVEADCOM	1
C513 ARRADCOM	1
C535 AVRADCOM/TSARCOM	1
C539 TRASANA	1
Q592 FSTC	4
Q619 MSIC REDSTONE	1
Q008 NTIC	1
Q043 AFMIC-IS	1
E404 AEDC/DOF	1
E410 AFDTC/IN	1
E429 SD/IND	1
P005 DOE/ISA/DDI	1
1051 AFIT/LDE	1
P090 NSA/CDB	1

Microfiche Nbr: FTD96C000002
NAIC-ID(RS)T-0516-95